Spectral and modal representations of the Doppler-shifted field in ocean waveguides

Henrik Schmidt
Massachusetts Institute of Technology, Cambridge, Massachusetts 02139

W. A. Kuperman[a)]
Scripps Institute of Oceanography, La Jolla, California 92093

(Received 2 September 1993; accepted for publication 26 January 1994)

A simple spectral representation is derived for the Doppler-shifted field in general stratified waveguides, including those with elastic bottoms and ice covers. By transforming the field representation for a moving, finite bandwidth source into the moving receiver's frame of reference, a spectral integral representation is obtained for the dynamic transfer functions, which may then be transformed into time domain responses by standard Fourier synthesis. The spectral representation of the Doppler-shifted field is more general than earlier modal formulations since it is not based on any assumptions concerning the invariance of mode shapes, and it properly accounts for modal cutoff effects. However, it will be demonstrated that its approximate modal expansion is consistent with earlier modal formulations. The spectral formulation has been implemented in an existing wave-number integration code, and applied to illustrate the fundamental physics of the source/receiver dynamics in stratified waveguides. Examples include moving source/receivers in shallow water, and the acoustic emission produced by propagating ice fractures in the Arctic.

PACS numbers: 43.30.Bp, 43.30.Es, 43.30.Ma

INTRODUCTION

It is well known that a moving source and/or receiver in free space results in a frequency Doppler shift which is described by the simple relation obtained from a Galilean transformation.[1] In a waveguide or stratified environment, source/receiver motion results in a more complicated Doppler structure because of multipath phenomena. The significance of the Doppler shift to sonar processing is well established, and the issue of modeling and understanding the complications introduced by the waveguide has therefore received some attention in the literature. The most general approach to modeling the Doppler shift is to use time-domain convolution, allowing for treatment of arbitrary source signatures and complex source/receiver dynamics.[2] However, this approach is computationally intensive and further the mathematical formulation does not directly reveal the waveguide physics. In contrast, representations in terms of normal modes have a direct connection to the fundamental waveguide physics, and have therefore been the methods of choice in most past modeling efforts addressing the fundamental physics of the waveguide Doppler phenomenon. Examples are the work of Guthrie *et al.*[3] who derived a modal expansion formulation of the Doppler-shifted field arising from a monochromatic source, moving radially relative to the receiver. Hawker[4] presented a more general modal formulation, expanding the field in a full Fourier–Bessel representation including the effect of azimuthal motion. Such earlier works have focused on the moving source, but as we will demonstrate here, the source/receiver dynamics is inherently nonreciprocal, with the moving receiver entering the formulation differently from the way the source dynamics appears. Further, such works have been using asymptotic expansions valid only for slow source/receiver motions, ignoring effects such as frequency dependence of mode shape and modal cutoff. Clearly, such approximations are valid for many sonar scenarios, but as we will demonstrate later by examples, there are problems arising in ocean acoustics where such approximations are inadequate. Recently, a simpler modal formulation was derived by Fawcett and Maranda,[5] and applied to address signal processing issues in dynamic scenarios. However, their approach only considers the relative source/receiver motion, and therefore ignores the effect of the joint motion through the medium, which, as will be clear from the present formulation and also from that of Hawker,[4] results in a Doppler shift in wave number, affecting the modal interference pattern.

We will here derive a spectral or wave-number integral representation of the Doppler-shifted field in stratified ocean environments, incorporating both source and receiver motion and providing a more complete representation of the Doppler effects than the modal formulations. On the other hand, a formulation in terms of normal modes has clear interpretational advantages, and we will therefore also derive a modal formulation through an eigenfunction expansion of the wave-number integration kernel.

Another important difference is that the present formulation is derived for sources of limited bandwidth. In combination with a transformation into the receiver's frame of reference, both spatially and in terms of frequency, this leads to an extremely simple result, where the Doppler effects are incorporated by almost trivial changes to the equivalent static formulation. The modal approximation becomes equally simple and easy to interpret physically, a fact which

[a)]Work initiated while at Naval Research Laboratory, Washington, DC 20375.

 0001-4966/94/96(1)/386/10/$6.00

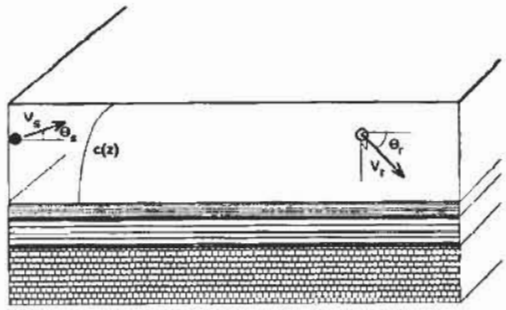

FIG. 1. Horizontally stratified ocean environment with source and receiver moving with velocity vectors $\mathbf{v}_s$ and $\mathbf{v}_r$, respectively.

allows for an heuristic extension to adiabatic mode theory.

We first describe the mathematical derivation of the spectral representation, followed by the derivation of the modal approximation, which directly allows for physical interpretation. An existing wave-number integration code has been straightforwardly modified to incorporate the source/receiver dynamics, and applied to illustrate the fundamental physics associated with moving sources and receivers in a shallow water environment. As a second example, we consider the acoustic emission produced by propagating fractures in an Arctic ice cover. This problem is of importance to the use of acoustic remote sensing of ice mechanical processes, but more importantly in the present context, it is characterized by very dramatic Doppler effects due to the high fracture speeds and the presence of slow seismic ice modes, leading to modal change and cutoff phenomena not described by the classical modal representations.

I. MATHEMATICAL FORMULATION

Assume an acoustic source is moving horizontally at depth z_s in a plane stratified ocean with velocity vector $\mathbf{v}_s$, as illustrated in Fig. 1. Similarly the receiver at depth z is moving with velocity vector $\mathbf{v}_r$. The angles between the velocity vectors and the radial vector connecting source and receiver are denoted θ_s and θ_r. We start with the wave equation governing the field produced by the moving source. As we will see later, once the expression for the field is found for the moving source, it is straightforwardly modified to incorporate the receiver motion. The wave equation in Cartesian coordinates, with the right-hand side representing a harmonic point source of time dependence $\exp(-i\Omega t)$ moving with a constant horizontal velocity vector $\mathbf{v}_s$, is

$$\nabla^2\psi(\mathbf{r},z,t)-\frac{1}{c^2}\frac{\partial^2\psi(\mathbf{r},z,t)}{\partial t^2}=-\delta(\mathbf{r}-\mathbf{v}_s t)\,\delta(z-z_s)e^{-i\Omega t}, \tag{1}$$

where ψ represents either the acoustic pressure or a wavefield potential. Introducing the Fourier transform pair,

$$f(t)=\frac{1}{2\pi}\int_{-\infty}^{\infty} f(\omega)e^{-i\omega t}\,d\omega, \tag{2}$$

$$f(\omega)=\int_{-\infty}^{\infty} f(t)e^{i\omega t}\,dt, \tag{3}$$

and applying Eq. (3) to Eq. (1), we arrive at the inhomogeneous *Helmholtz equation*,

$$(\nabla^2+k_\omega^2)\psi(\mathbf{r},z,\omega)=-\delta(z-z_s)\int \delta(\mathbf{r}-\mathbf{v}_s t)\times e^{i(\omega-\Omega)t}\,dt, \tag{4}$$

where k_ω is the medium wave number at frequency ω, $k_\omega=\omega/c$.

A. Wave-number integral representation

Because of the source motion, we do not assume the problem to be axisymmetric; rather than the Hankel transforms usually used for a stationary point source, we use a two-dimensional Fourier transform to reduce the spatial dimension of the Helmholtz equation. Thus we use the transform pair,

$$\psi(\mathbf{r},z;\omega)=\int d^2\mathbf{k}_r\,\psi(\mathbf{k}_r,z;\omega)e^{i\mathbf{k}_r\cdot\mathbf{r}}, \tag{5}$$

$$\psi(\mathbf{k}_r,z;\omega)=\frac{1}{(2\pi)^2}\int d^2\mathbf{r}\,\psi(\mathbf{r},z;\omega)e^{-i\mathbf{k}_r\cdot\mathbf{r}}, \tag{6}$$

to transform Eq. (4) into the *depth-separated wave equation*,

$$\frac{d^2\psi(\mathbf{k}_r,z;\omega)}{dz}+(k_\omega^2-k_r^2)\psi(\mathbf{k}_r,z;\omega)$$
$$=-\frac{\delta(z-z_s)}{(2\pi)^2}\int e^{i(\omega-\Omega-\mathbf{k}_r\cdot\mathbf{v}_s)t}\,dt$$
$$=-\frac{\delta(z-z_s)}{2\pi}\,\delta(\omega-\Omega-\mathbf{k}_r\cdot\mathbf{v}_s), \tag{7}$$

with $k_r=|\mathbf{k}_r|$, and where we have used the identities,

$$\int d^2\mathbf{r}\,\delta(\mathbf{r}-\mathbf{v}_s t)e^{-i\mathbf{k}_r\cdot\mathbf{r}}=e^{-\mathbf{k}_r\cdot\mathbf{v}_s t}, \tag{8}$$

and

$$\frac{1}{2\pi}\int e^{i(\omega-\Omega-\mathbf{k}_r\cdot\mathbf{v}_s)t}\,dt=\delta(\omega-\Omega-\mathbf{k}_r\cdot\mathbf{v}_s). \tag{9}$$

Equation (7) is a standard depth-separated wave equation, with the solution

$$\psi(\mathbf{k}_r,z;\omega)=\delta(\omega-\Omega-\mathbf{k}_r\cdot\mathbf{v}_s)G(k_r,z;\omega), \tag{10}$$

where $G(k_r,z;\omega)$ is the depth-dependent Green's function for the waveguide at frequency ω, which may be determined for arbitrary stratifications by one of the standard methods applied in wave-number integration codes such as SAFARI.[6,7]

The time domain solution then follows by applying the inverse Fourier transforms in Eqs. (5) and (2),

$$\psi(\mathbf{r},z,t)=\frac{1}{2\pi}\int d\omega\,e^{-i\omega t}\int d^2\mathbf{k}_r\,\psi(\mathbf{k}_r,z,\omega)e^{i\mathbf{k}_r\cdot\mathbf{r}}, \tag{11}$$

which by inserting Eq. (10) reduces to

$$\psi(\mathbf{r},z,t)=\frac{1}{2\pi}\int d^2\mathbf{k}_r\,G(k_r,z;\Omega+\mathbf{k}_r\cdot\mathbf{v}_s)\times e^{-i[(\Omega+\mathbf{k}_r\cdot\mathbf{v}_s)t-\mathbf{k}_r\cdot\mathbf{r}]}. \tag{12}$$

The frequency term appearing in both the kernel and the exponential in Eq. (12), i.e.,

$$\omega=\Omega+\mathbf{k}_r\cdot\mathbf{v}_s, \tag{13}$$

represents the *Doppler frequency shift* for each wave-number component of the field resulting from a moving harmonic source. Now it is clear, that since the expression in Eq. (12) represents the field at all range vectors $\mathbf{r}$, we can straightforwardly modify it to include the receiver motion. Thus the range vector for a receiver at position $\mathbf{r}_0$ at time $t=0$, and moving with a velocity vector $\mathbf{v}_r$, is given by $\mathbf{r}=\mathbf{r}_0+\mathbf{v}_r t$, which inserted in Eq. (12) yields,

$$\psi(\mathbf{r}_0+\mathbf{v}_r t,z,t)=\frac{1}{2\pi}\int d^2\mathbf{k}_r\, G(k_r,z;\Omega+\mathbf{k}_r\cdot\mathbf{v}_s)\times e^{-i\{[\Omega+\mathbf{k}_r\cdot(\mathbf{v}_s-\mathbf{v}_r)]t-\mathbf{k}_r\cdot\mathbf{r}_0\}}. \tag{14}$$

Here, it is interesting to note the asymmetry between source and receiver motion. Thus, whereas both source and receiver motion yield a frequency shift through the exponential, only the source motion affects the integration kernel, the depth-dependent Green's function. Therefore, reciprocity does not hold for moving sources and receivers. Also note that, as expected, no frequency Doppler shift is observed if source and receiver are moving at identical velocities, but the kernel is still affected, in a nonreciprocal way. Therefore, the field observed at a receiver moving with the same speed and direction as the source is different from the field observed in the stationary case, a fact which is rarely appreciated when interpreting experimental data. On the other hand, as we shall demonstrate, this effect is rather small, making the static approximation valid for most realistic source/receiver motions. A joint source/receiver motion is clearly equivalent to stationary sources and receivers in a moving medium.

Even though Eq. (14) represents the field through a wave-number integral, this expression is not well suited for direct numerical implementation. The reason is that the source/receiver dynamics couples the time and wave number through the argument to the exponential function, requiring the integral to be evaluated for each individual time value. Furthermore, these expressions refer to a harmonic excitation. In reality, the source will always have a finite bandwidth, and the field at the receiver is therefore given as a Fourier integral of the above expressions. Thus, for a source spectrum $S(\Omega)$, Eq. (14) changes to

$$\psi(\mathbf{r}_0+\mathbf{v}_r t,z,t)=\frac{1}{4\pi^2}\int d\Omega\, S(\Omega)\int d^2\mathbf{k}_r\times G(k_r,z;\Omega+\mathbf{k}_r\cdot\mathbf{v}_s)e^{-i\{[\Omega+\mathbf{k}_r\cdot(\mathbf{v}_s-\mathbf{v}_r)]t-\mathbf{k}_r\cdot\mathbf{r}_0\}}. \tag{15}$$

In the receiver's frame of reference the frequency spectrum of the field at the receiver now follows by applying the Fourier transform in Eq. (3) to Eq. (15):

$$\begin{aligned}\psi(\mathbf{r}_0+\mathbf{v}_r t,z,\omega)&=\int dt\, e^{i\omega t}\psi(\mathbf{r}_0+\mathbf{v}_r t,z,t)\\&=\frac{1}{4\pi^2}\int d\Omega\, S(\Omega)\int d^2\mathbf{k}_r\, e^{i\mathbf{k}_r\cdot\mathbf{r}_0}G(k_r,z;\Omega+\mathbf{k}_r\cdot\mathbf{v}_s)\int dt\,\exp-i[\Omega-\omega+\mathbf{k}_r\cdot(\mathbf{v}_s-\mathbf{v}_r)]t\\&=\frac{1}{2\pi}\int d^2\mathbf{k}_r\, e^{i\mathbf{k}_r\cdot\mathbf{r}_0}\int d\Omega\, S(\Omega)G(k_r,z;\Omega+\mathbf{k}_r\cdot\mathbf{v}_s)\delta[\Omega-\omega+\mathbf{k}_r\cdot(\mathbf{v}_s-\mathbf{v}_r)]\\&=\frac{1}{2\pi}\int d^2\mathbf{k}_r\, e^{i\mathbf{k}_r\cdot\mathbf{r}_0}S(\Omega_k)G(k_r,z;\omega+\mathbf{k}_r\cdot\mathbf{v}_r),\end{aligned} \tag{16}$$

where Ω_k is the Doppler-shifted source frequency,

$$\Omega_k=\omega-\mathbf{k}_r\cdot(\mathbf{v}_s-\mathbf{v}_r). \tag{17}$$

Equation (16) represents stationary frequency components of the field in the receiver's frame of reference, with the time-domain response following by evaluation of the inverse Fourier transform in Eq. (2). Thus simply by transforming into the receiver's frame of reference, i.e., changing from a representation in terms of "source frequency" Ω in Eq. (15) to a representation in terms of "receiver frequency" ω, we have eliminated the coupling between time and wave number. As a result, the wave number and frequency integrations are performed independently, as in the static case. In fact, the differences introduced by the dynamics are rather trivial. The first concerns the source spectrum $S(\Omega_k)$ which is wave-number independent in the static case and therefore in that case may be applied outside the wave-number integral, as part of the Fourier synthesis; the other difference is the change in frequency argument to the depth-dependent Green's function. We will later discuss the physical significance of these differences.

In spite of its extraordinary simplicity, Eq. (16) is *exact* within the limitations of the linear theory of acoustics. Thus the only assumption made is that source and receiver are moving at constant speed.

Unfortunately, the evaluation of the two-dimensional wave-number integral in Eq. (16) is computationally intensive. However, in underwater acoustics the range separation of the source and receiver is usually large compared to the track of each during the time duration of the signal. The

angles θ_s and θ_r between the velocity vectors of the source and receiver, respectively, and the radial vector connecting them, can therefore be considered constant, and we can replace the 2D Fourier integral in Eq. (16) by a Hankel transform representation in the horizontal wave number,[8] i.e.,

$$\psi(\mathbf{r}_0+\mathbf{v}_r t,z,\omega)\simeq\int_0^\infty dk_r\, k_r J_0(k_r r_0)S(\Omega_k) \times G(k_r,z;\omega+k_r v_r\cos\theta_r) = \frac{1}{2}\int_{-\infty}^{\infty} dk_r\, k_r H_0^{(1)}(k_r r_0)S(\Omega_k) \times G(k_r,z;\omega+k_r v_r\cos\theta_r), \quad (18)$$

with

$$\Omega_k=\omega-k_r(v_s\cos\theta_s-v_r\cos\theta_r). \quad (19)$$

Using this approximation, it is extremely simple to modify an existing wave-number integration code as SAFARI[6,7] to compute the Doppler-shifted acoustic field. The only change needed is to compute the depth-dependent Green's function at the shifted frequency $\omega+k_r v_r\cos\theta_r$ for every wave number k_r considered, and multiply it by the source spectrum at the shifted frequency Ω_k. The resulting dynamic transfer functions are then transformed into the time-domain response by standard Fourier synthesis.

B. Normal-mode representation

Based on the spectral representations given above, it is now straightforward to proceed to the normal-mode representation of the Doppler-shifted discrete part of the acoustic field. Ignoring the branch line contribution, the depth-dependent Green's function can be written in terms of normal modes,[9]

$$G(k_r,z;\omega)\simeq\frac{1}{2\pi\rho(z_s)}\sum\frac{\Psi_n(z)\Psi_n(z_s)}{k_r^2-k_n^2}, \quad (20)$$

where k_n are the eigenvalues of the homogeneous form of Eq. (7), and Ψ_n are the associated eigenvectors. We can now replace the kernel in Eq. (18) by the modal expansion in Eq. (20), but with the wave number k_n replaced by the eigenvalues k_n^* at Doppler-shifted frequency $\omega+k_r v_r\cos\theta_r$, i.e., for $v_r/c\ll 1$,

$$k_n^*\simeq k_n\left(1+v_r\cos\theta_r\frac{dk_n}{d\omega}\right)=k_n\left(1+\frac{v_r}{v_{ng}}\cos\theta_r\right), \quad (21)$$

where v_{ng} is the *group velocity* of the nth mode at angular frequency ω. The wave-number integral in Eq. (18) can then, in analogy to the static case, be replaced by the modal sum,

$$\psi(\mathbf{r}_0+\mathbf{v}_r t,z,\omega)\simeq\frac{i}{4\rho(z_s)}\sum_n S(\Omega_n)\Psi_n(z)\Psi_n(z_s)H_0^{(1)} \times\left[k_n r_0\left(1+\frac{v_r}{v_{ng}}\cos\theta_r\right)\right], \quad (22)$$

where

$$\Omega_n=\omega-k_n(v_s\cos\theta_s-v_r\cos\theta_r)=\omega\left(1-\frac{v_s}{v_{np}}\cos\theta_s+\frac{v_r}{v_{np}}\cos\theta_r\right), \quad (23)$$

with $v_{np}=\omega/k_n$ being the modal *phase velocity*. Here, it has been assumed that the change in modal eigenfunctions is negligible. Further, this expression ignores any modal cutoff effects introduced by the Doppler shift, and as such Eq. (22) represents another level of approximation compared to the spectral representation in Eq. (18). On the other hand, the physical interpretation of the dynamic effects is very simple in the modal approximation. It is clear from Eq. (23) that the Doppler shift in observed frequency is associated with the horizontal phase velocity of the individual modes. Since each mode is a result of the constructive interference of up- and down-going plane waves with distinct grazing angles $\phi_n=\cos^{-1}(k_n/k_w)$, different modes clearly have different phase velocities and therefore different Doppler shifts.

The source/receiver dynamics also yields a perturbation in the interference associated with the change in the modal propagation wave numbers in Eq. (21). It is clear from Eq. (22) that this change in modal eigenvalue can alternatively be interpreted as a change in range. With this observation, we can interpret this effect physically as being associated with the different distances the modes are traveling from being launched at the source to being received at the receiver, due to their different *group velocities*. Here, it is interesting to note that this effect only involves the receiver motion. However, this asymmetry, which is the reason for the earlier discussed lack of reciprocity, actually makes sense physically. Assume the source function is a delta function in time, i.e., $S(\Omega)=1$. All modes in the waveguide will then be excited at the same instance in time, and their arrival time and therefore relative phase will be unaffected by the continued source motion. Therefore, if the receiver is at rest, the arrival time, and therefore relative phase, of the modes is independent of the source dynamics. On the other hand, if the receiver is moving, it will pick up the individual modal arrivals at different points in space due to their different group velocities. As a result, the relative phase between the modes is affected, reflected through the change in observed modal wave number given in Eq. (21). This *wavenumber Doppler shift* was ignored in the formulation of Fawcett and Maranda,[5] but as is clear from Eqs. (22) and (23), this effect can be equally important to the *frequency Doppler shift*, depending on the ratio between the relative source/receiver speed and the receiver speed itself.

It is easily verified, that for a stationary receiver and a moving, monochromatic source, $S(\Omega)=\delta(\Omega-\Omega_0)$, the Fourier transform of Eq. (23) becomes identical to the expressions derived by Guthrie *et al.*[3] and Hawker[4] for this special case. Their results could also be derived by directly replacing the wave-number integral in Eq. (12) by its modal expansion.

Although here we are primarily concerned with range-independent scenarios, we will derive a simple modification of the adiabatic mode expansion, incorporating the source/receiver dynamics. This is easily done heuristically, based on

the physical interpretation of the two effects of the dynamics stated above. For the static case the adiabatic expansion is of the form,[9]

$$\psi(r,z,\omega)\simeq\frac{iS(\omega)}{\rho(z_s)\sqrt{8\pi}}\,e^{-i\pi/4}\times\sum_n \Psi_n(z)\Psi_n(z_s)\,\frac{e^{i\int_0^r k_n(r')dr'}}{\sqrt{\int_0^r k_n(r')dr'}}. \tag{24}$$

Now it is clear from the above that the frequency Doppler shift depends on the phase velocities at the source and receiver, whereas the phase shift is associated with the different ranges the modes are traveling before reaching the moving receiver. Based on this observation, the adiabatic result directly follows as

$$\psi(r_0+v_r t,z,\omega)\simeq\frac{i}{\rho(z_s)\sqrt{8\pi}}\,e^{-i\pi/4}\times\sum_n S(\Omega_n^*)\Psi_n(z)\Psi_n(z_s)\,\frac{e^{i\int_0^{r_n^*} k_n(r')dr'}}{\sqrt{\int_0^{r_n^*} k_n(r')dr'}}, \tag{25}$$

where

$$\Omega_n^*=\omega\left(1-\frac{v_s}{v_{np}(0)}\cos\theta_s+\frac{v_r}{v_{np}(r_0)}\cos\theta_r\right), \tag{26}$$

and r_n^* are the perturbed ranges for the phase integrals,

$$r_n^*=r_0\left(1+\frac{v_r}{v_{ng}(r_0)}\cos\theta_r\right). \tag{27}$$

The modification of existing normal-mode codes to account for the source/receiver dynamics is clearly equally simple as the one described above for wave-number integration codes.

II. NUMERICAL EXAMPLES

The key results of this paper are the extraordinarily simple expressions for the dynamic transfer functions in Eqs. (16), (18), and (22). As described above, these equations represent the dynamic field at increasing levels of approximation. The exact representation in Eq. (16) clearly is the most general. However, it involves the computationally intensive task of evaluating a two-dimensional Fourier transform. However, in most cases of interest in underwater acoustics the source and receiver are of wide separation, allowing for the use of the simpler Hankel transform representation in Eq. (18). This representation of the dynamic field is compatible with standard wave-number integration codes, and we have therefore modified SAFARI[6,7] accordingly. Clearly, we could have used a modal code instead, together with Eq. (22), but, as described above, this would eliminate the effects of changing mode shape and modal cutoff, which may be important as we will see in the following examples.

As described above, the source/receiver dynamics has two fundamental effects. One is the frequency Doppler shift associated with the ratio between the relative velocity of the source and receiver and the individual modal *phase velocities*. The other effect is a phase shift accounting for the different total propagation paths of the modes, and therefore associated with the ratio of the receiver speed to the modal *group velocities*. Both of these effects must be considered when using sonar systems in dynamic scenarios since they will affect the performance of the processing system. In a later paper, we will address such processing effects, but here we will use a few examples to illustrate the basic physics of the dynamic source/receiver scenario.

A. Shallow-water scenario

Here, we consider an omnidirectional source and receiver moving at constant speeds in the shallow-water environment shown in Fig. 2, consisting of a water column of depth 100 m, with a downward-refracting summer profile, and a homogeneous limestone bottom with compressional speed 2500 m/s, shear speed 800 m/s, and density 2200 kg/m^3. The water is assumed to be lossless, whereas the attenuations in limestone are assumed to be 0.1 and 0.2 dB/λ for compression and shear, respectively. The source and receiver depths are $z_s=30$ m and $z=55$ m, respectively.

First, we will consider the case where both source and receiver are propagating with the same speed and direction.

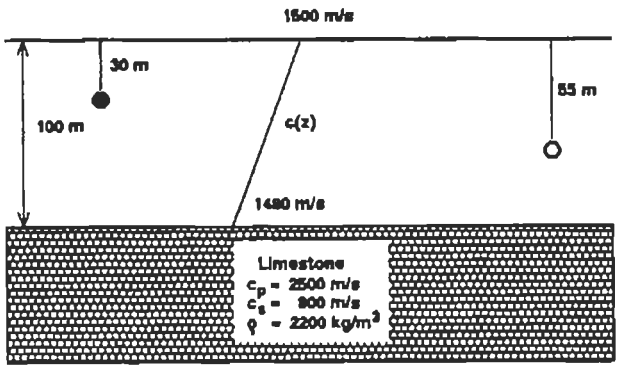

FIG. 2. Shallow-water environment with water depth 100 m. The bottom consists of an infinite limestone half-space with compressional speed 2500 m/s, shear speed 800 m/s, and density 2200 kg/m^3. The source depth is 30 m and the receiver depth 55 m.

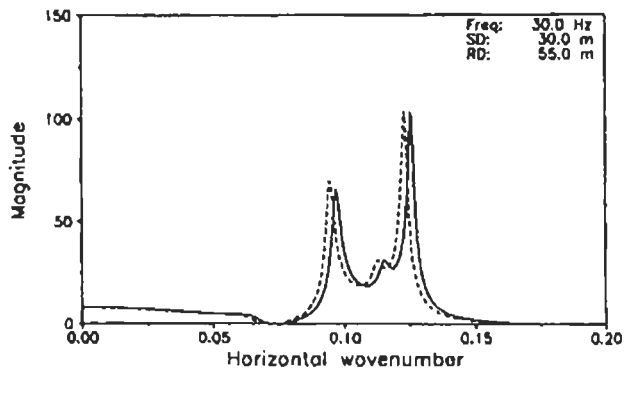

FIG. 3. Depth-dependent Green's function $G(k_r,z;\omega+k_r v_r\cos\theta_r)$ for source and receiver both moving at 30 m/s (solid curve) and for stationary source and receiver (dashed curve).

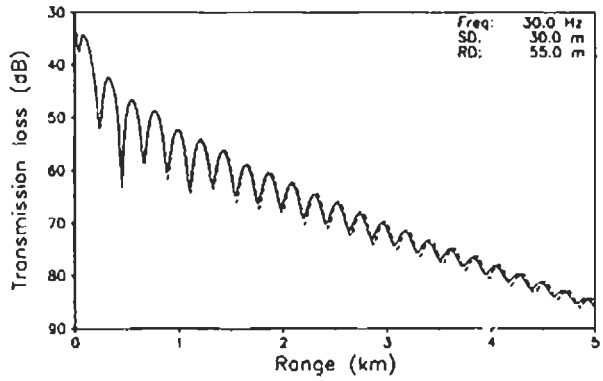

FIG. 4. Transmission loss versus range separation for source and receiver both moving at 30 m/s (solid curve) and for stationary source and receiver (dashed curve).

In this case, there will be no frequency Doppler shift, but as described above, there will still be a shift in modal phase to be accounted for. To emphasize the physical effects, we assume the source and receiver to be moving along the same track at the rather unrealistic speed of $v_s = v_r = 30$ m/s (60 knots). Figure 3 shows the associated integration kernel $G(k_r, z; \omega + k_r v_r \cos\theta_r)$ for source frequency 30 Hz as a solid curve. The corresponding result for the static case is indicated by the dashed curve. Three modes are excited at this frequency, but for this source/receiver combination modes 1 and 3 clearly dominate the kernel, and it is also evident that the kernel is affected by the source/receiver dynamics. Although not obvious from Fig. 3, modes 1 and 3 are shifted differently in wave numbers, and the associated field will therefore have a change in modal interference pattern. This is illustrated in Fig. 4 in terms of transmission loss versus range. Clearly, the effect is weak for the short ranges considered here, even for the high speed considered. However, the effect increases with range, and the implication for use of high-resolution matched-field processing concepts can be expected to be more severe. This issue will be addressed in a later paper.

We will also use this shallow-water scenario to illustrate the nonreciprocity of source and receiver motion and its physical manifestation. This is most easily demonstrated in the time domain. We assume the source to emit a transient signal with center frequency 30 Hz and bandwidth 10 Hz.

First, we assume the source to be stationary, and the receiver to move away with a speed of 30 m/s. The initial range of the receiver is 5 km. The received signal is shown in Fig. 5(a) as a solid curve, and for comparison the corre-

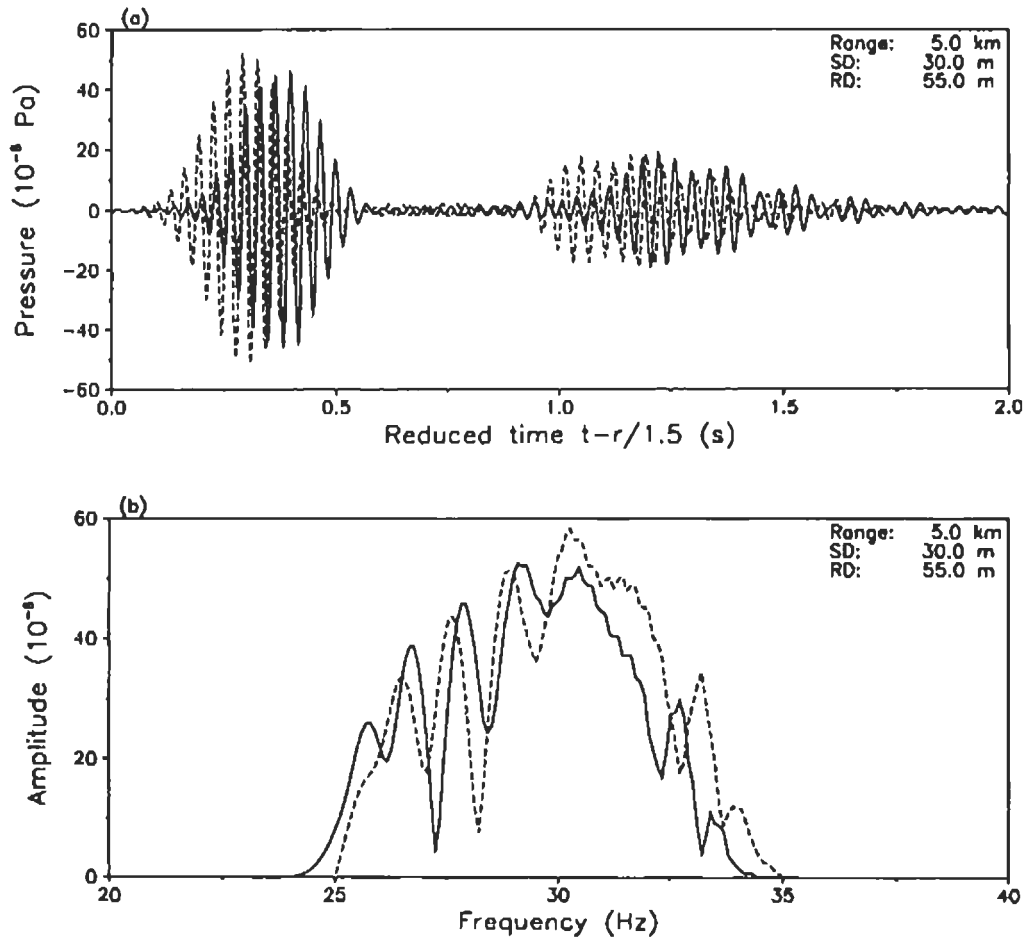

FIG. 5. Received signal for source signal of bandwidth 10 Hz and center frequency 30 Hz. Source depth is 30 m and receiver depth is 55 m. (a) Time series. (b) Frequency spectrum. Solid curves show results for receiver moving away from source at speed 30 m/s from an initial range of 5 km ($v_s = 0$ m/s, $v_r = 30$ m/s). Dashed curves show corresponding results for a stationary receiver at 5-km range.

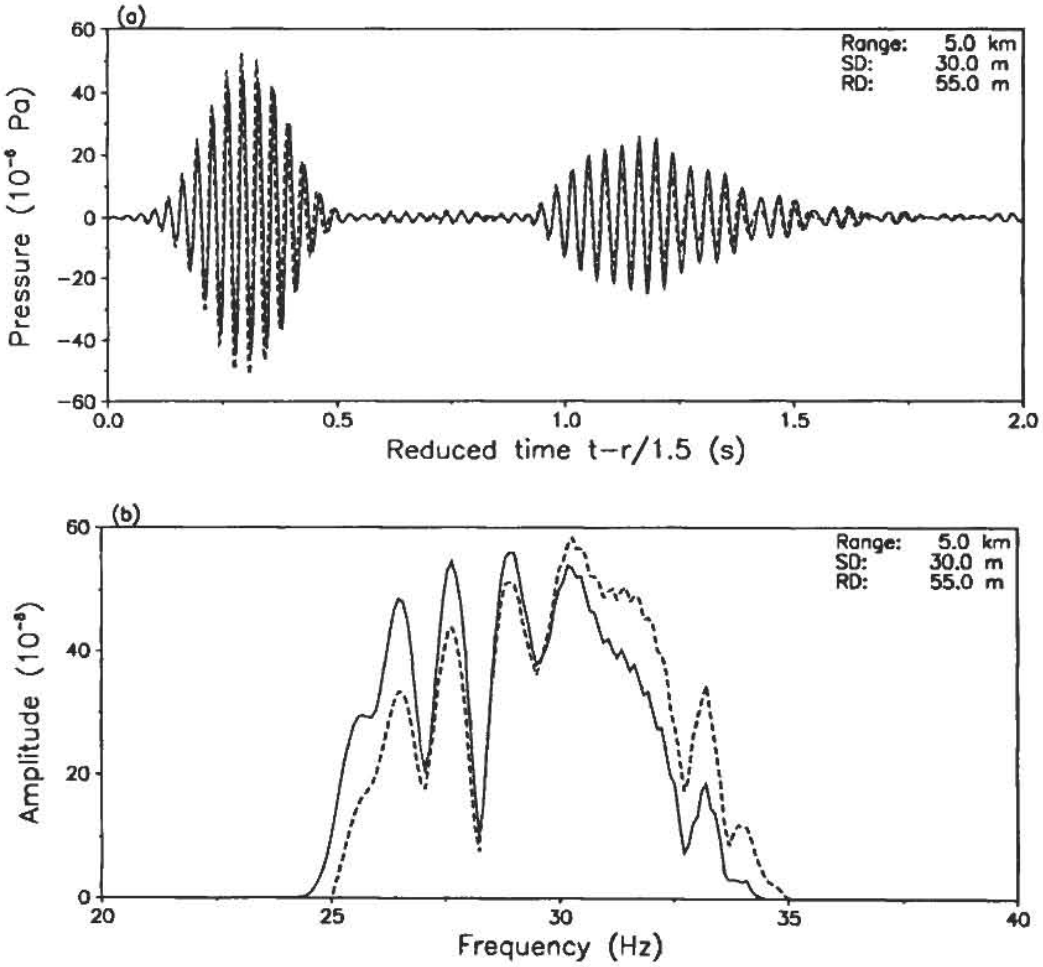

FIG. 6. Received signal for source signal of bandwidth 10 Hz and center frequency 30 Hz. Source depth is 30 m and receiver depth is 55 m. (a) Time series. (b) Frequency spectrum. Solid curves show results for source moving away from receiver at speed 30 m/s from an initial range of 5 km ($v_s=-30$ m/s, $v_r=0$ m/s). Dashed curves show corresponding results for a stationary source at 5-km range.

sponding result for the static scenario is indicated by the dashed curve. The first arrival is mode 1, and the receiver dynamics clearly yields a time delay due to the fact that the receiver is moving during the transit time of the mode. The second arrival is the interference of modes 2 and 3, with mode 3 dominating. It is evident that the dynamics here gives rise to a longer time delay than for mode 1, due to the lower group velocity of modes 2 and 3. In addition, the interference of modes 2 and 3 is changing, with a significant change in pulse shape as a result, compared to the static case. Figure 5(b) shows the associated frequency spectra of the received signals, and as expected there is a clear shift toward lower frequencies in the dynamic case. Here, a change in the modal interference is evident as well.

Next, we consider the same scenario, but now assuming the receiver to be stationary, and the source moving away at 30 m/s. The resulting timeseries and spectrum are shown in Fig. 6(a) and (b), respectively, where the solid curve again represents the dynamic result, and the dashed curve represent the static result. Clearly, the change introduced by the dynamics is much less dramatic here. The shape of the arrivals is virtually unchanged, except for a frequency Doppler shift, which is particularly evident in Fig. 6(b). An interesting effect, however, is the differences in modal excitation. Thus the amplitude of mode 1 is smaller in the dynamic case as would be expected due to the fact that the average source/receiver range is longer than in the static case. However, mode 3 is of higher amplitude than the static equivalent. The reason for this is the fact that the mode shapes are changing with frequency, and for this particular source/receiver combination, the lowering in frequency introduced by the Doppler shift will yield a higher excitation of mode 3, more than compensating the increasing mean range. Such an effect would not be properly modeled if we had used the modal expansion in Eq. (22) with its inherent assumption of invariance of mode shapes. The main point to stress, however, is the significant difference between the results in Figs. 5 and 6, clearly illustrating the lack of reciprocity.

B. Acoustic emission from ice fractures

As a second example, we consider the problem of recording acoustic emission from propagating fractures in an Arctic ice cover. This problem is of significant importance in relation to the use of acoustic remote sensing of ice mechanical processes, but it is also a particularly interesting physical

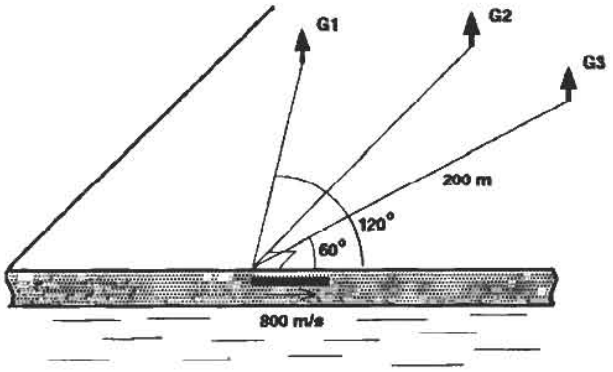

FIG. 7. Scenario for simulating geophone recording of acoustic emission from propagating tensile crack in the Arctic ice cover. The crack tip is assumed to be at a depth 1 m below the ice surface, and propagating with a horizontal speed of 800 m/s, over a total crack length of 16 m. The acoustic emission is detected by three vertical geophones at a range of 200 m from the crack initiation point, at bearings 120°, 90°, and 60° relative to to the crack propagation.

problem due to the interplay of high fracture speeds and low phase and group velocities of some of the dominant propagation modes in the ice cover.

To illustrate the dynamic fracture effects, we use a simple environmental model. Thus the ice cover is assumed to be a homogeneous and isotropic, elastic plate of a constant thickness of 4 m. The compressional and shear speeds are 3500 and 1800 m/s, respectively, and the density is 900 kg/m^3. The attenuations are assumed to be 0.5 and 1.0 dB/λ for compression and shear, respectively. Since we are here concerned about relatively short ranges and travel times, refraction in the water will be insignificant, and the water column is represented by an infinite half-space with constant sound speed 1438 m/s.

It is well established that the ice will support two fundamental modes that are never cutoff: the supersonic, and therefore leaky, *compressional mode*, and the subsonic *flexural mode*.[10] At high frequencies, the ice plate may support a large number of modes, with the cutoff frequency for

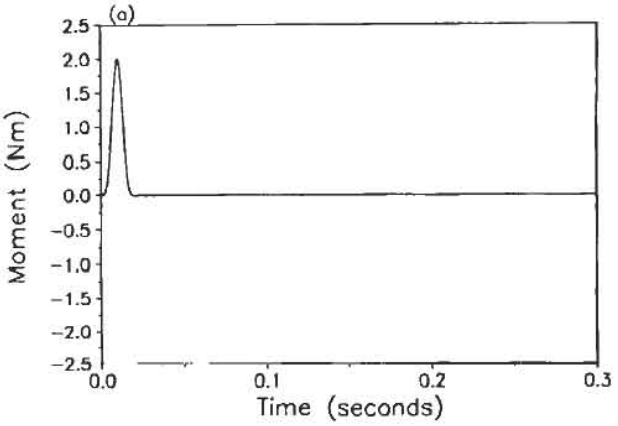

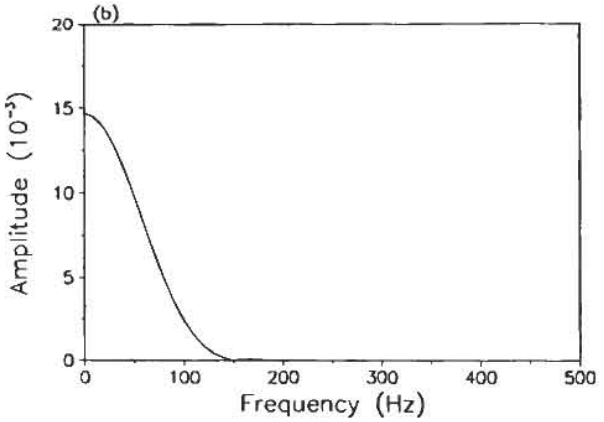

FIG. 8. Seismic moment representation of tensile crack. (a) Time series. (b) Frequency spectrum.

the first higher-order mode being approximately equal to the *thickness-shear frequency* for the plate,[10,11]

$$f_0 = c_s/2H, \tag{28}$$

where c_s is the shear speed and H is the ice thickness. For the present case, this translates into a cutoff frequency of f_0=225 Hz, below which only the two fundamental modes exist.

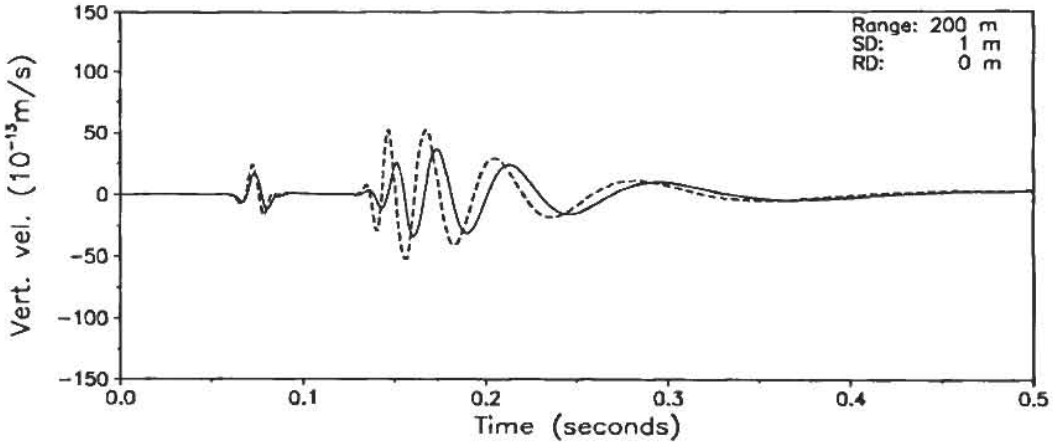

FIG. 9. Comparison of signals received on geophone G1 (solid curve) and geophone G2 (dashed curve). Relative to the receiver, the source is receding with radial velocity $v_s \cos\theta_s = -400$ m/s for G1, and 0 m/s for G2.

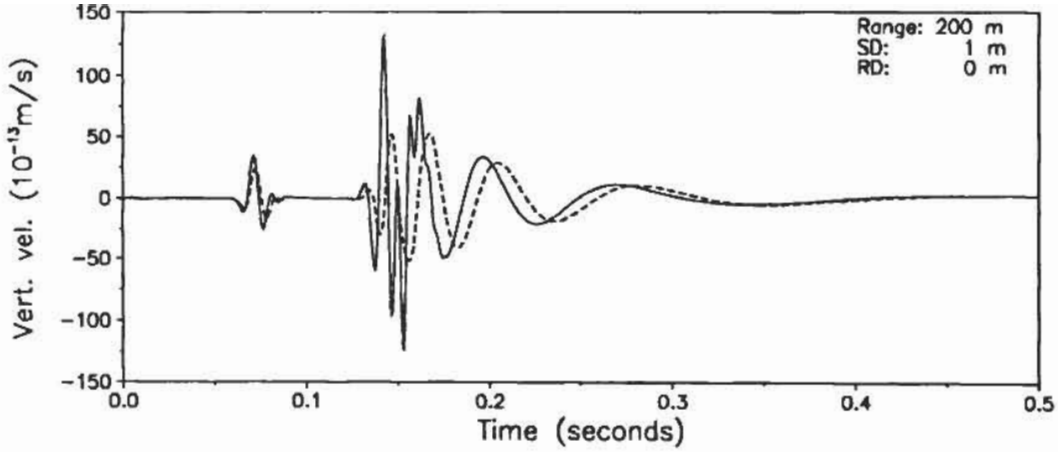

FIG. 10. Comparison of signals received on geophone G3 (solid curve) and geophone G2 (dashed curve). Relative to the receiver, the source is approaching with radial velocity $v_s \cos\theta_s = 400$ m/s for G3, and 0 m/s for G2.

We consider the scenario illustrated in Fig. 7. A tensile (e.g., thermal) crack is initiated at time $t=0$ s and propagates with a constant speed of 800 m/s for a total period of 20 ms, yielding a final crack length of 16 m. The acoustic emission is recorded by three vertical geophones, denoted G1, G2 and G3, placed at a range of 200 m from the crack initiation point, at bearings 120°, 90°, and 60°, respectively, relative to the fracture propagation direction.

The crack tip is represented by an omnidirectional seismic moment source, with a bell-shaped time dependence, as shown in Fig. 8(a). The associated frequency spectrum is shown in Fig. 8(b), indicating the dominant components to be at frequencies less than 150 Hz. This source representation is not necessarily realistic, but it contains all the fundamental physics necessary for illustrating the dynamic effects of the fracture propagation and the coupling to the ice modes.

Since the range to the receivers is large compared to the length of the crack, we will again use Eq. (18) to simulate the response. Figure 9 shows the resulting timeseries for geophones G1 (solid curve) and G2 (dashed curve). It is clear from the geometry in Fig. 8 that the crack tip is moving away from the receiver at a projected speed of 400 m/s, in our notation corresponding to $v_s \cos\theta_s = -400$ m/s, whereas within our approximations the source is at rest relative to geophone G2. A comparison of the two responses in Fig. 9 shows the expected frequency Doppler shifts, both for the fundamental *compressional mode* arriving at $t=0.06$ s, but much more clearly for the highly dispersive and slow fundamental *flexural mode* between $t=0.12$ s and $t=0.5$ s. Another effect is a decrease in the observed amplitudes, primarily due to the longer mean range for geophone G1.

Similarly, Fig. 10 shows a comparison of the response of geophones G3 (solid curve) and G2 (dashed curve). For geophone G3, the crack tip is approaching with a projected speed of 400 m/s, i.e., $v_s \cos\theta_s = 400$ m/s, and here the difference is obviously much more dramatic than for G1. We clearly observe the expected effects of upward Doppler shift and higher amplitudes for both fundamental modes. However, in addition we see a distinct high-frequency arrival interfering with the initial phase of the fundamental flexural wave. This is due to the excitation of a higher-order mode in the ice. As described above, the cutoff frequency for the first higher-order mode is 225 Hz. As a result, this mode was not observed on geophone G1 and G2 due to the fact that the source contains energy only up to 150 Hz, and the signal on G2 has negative Doppler shift. However, the relatively low-phase velocity of the higher-order mode, in combination with the high-source speed, will produce a positive Doppler shift in the forward direction, large enough to allow for its excitation, and therefore detection by geophone G3. This effect would clearly not be included in a modal expansion, ignoring cutoff effects and changes in mode shape.

III. CONCLUSION

We have derived a simple spectral formulation of the Doppler-shifted field in general, stratified waveguides, including elastic bottoms and ice covers. By transforming the response for finite bandwidth sources into the moving receiver's frame of reference, the resulting spectral representation appears as an almost trivial modification of the static equivalent. By approximating the spectral kernel by its eigenfunction expansion, an equally simple modal representation was obtained, particularly well suited for physical interpretation, and demonstrating the consistency with earlier modal derivations. However, the spectral representation is more general than the modal formulations since it does not include any assumptions concerning the invariance of mode shapes, and properly accounts for modal cutoff effects. The derived formulations are easily incorporated in existing propagation models, allowing for numerical evaluation of the Doppler-shifted field at virtually no additional computational cost, compared to the static case. We have implemented the spectral formulation in an existing wave-number integration code, and used it to illustrate the fundamental physics of the source/receiver dynamics in stratified waveguides, including shallow-water and Arctic environments.

ACKNOWLEDGMENTS

This work was supported in part by the Office of Naval Research, Arctic Program Office.

[1] A. D. Pierce, *Acoustics: An Introduction to Its Physical Principles and Applications* (American Institute of Physics, Woodbury, NY, 1989).

[2] K. V. Rao, T. M. Michaud, and H. Schmidt, "Doppler shifts in underwater acoustics using field solutions," OCEANS-91, IEEE Proc., Honolulu, HI, 1991.

[3] A. N. Guthrie, R. M. Fitzgerald, D. A. Nutile, and J. D. Shaffer, "Long-range low-frequency cw propagation in the deep ocean: Antigua-Newfoundland," J. Acoust. Soc. Am. **56**, 58–64 (1974).

[4] K. E. Hawker, "A normal mode theory of acoustic Doppler effects in the oceanic waveguides," J. Acoust. Soc. Am. **65**, 675–681 (1979)

[5] J. A. Fawcett and B. H. Maranda, "A hybrid target motion analysis/matched-field processing localization method," J. Acoust. Soc. Am. **94**, 1363–1371 (1993).

[6] H. Schmidt and F. B. Jensen, "A full wave solution for propagation in multilayered viscoelastic media with application to Gaussian beam reflection at fluid–solid interfaces," J. Acoust. Soc. Am. **77**, 813–825 (1985).

[7] H. Schmidt and G. Tango, "Efficient global matrix approach to the computation of synthetic seismograms," Geophys. J. R. Astron. Soc. **84**, 331–359 (1986).

[8] P. M. Morse and K. U. Ingard, *Theoretical Acoustics* (Princeton U.P., Princeton, NJ, 1968), pp. 364–365.

[9] F. B. Jensen, W. A. Kuperman, M. B. Porter, and H. Schmidt, *Computational Ocean Acoustics* (American Institute of Physics, Woodbury, NY, 1994).

[10] B. E. Miller and H. Schmidt, "Observation and inversion of seismo-acoustic waves in a complex Arctic ice environment," J. Acoust. Soc. Am. **89**, 1668–1685 (1991).

[11] R. D. Mindlin, *An Introduction to Mathematical Theory of Vibration of Elastic Plates* (Fort Monmouth, NY U.S. Army Signal Corps. Engineering Laboratories, 1955).